ChemCatChem

Research Article
doi.org/10.1002/cctc.202201015

Europe
European Chemical
Societies Publishing

www.chemcatchem.org

Oxygen On-Demand: Understanding the Oxygen Reduction Reaction (ORR) Performance Enhancement of Conductive Polymer Films upon Modification with ZIF-8 MOF

Federico C. D. López,[a] Andrés I. Bertoni,[b] Juan A. Allegretto,[a] Waldemar A. Marmisollé,[a] Omar Azzaroni,[a] Matías Rafti,*[a] and Doris Grumelli*[a]

Recent developments surrounding the oxygen reduction reaction (ORR) focus on low-cost alternatives to materials used in traditional electrodes, e.g. Pt. To accumulate competitive advantages, these non-traditional electrodes often consist of multiple functional coating layers. Considering that each layer can potentially alter the reaction mechanism, thus changing its technological value, it becomes relevant to study how a particular electrode architecture impacts on the considered reaction pathway. From kinetic studies with rotating disk electrodes (RDE) it was found that, for Au electrodes coated with the conductive polymer P(ABA–ANI), either bare or modified with ZIF-8 (MOF) microcrystals, the ORR occurs (at neutral pH) via an associative pathway, involving a two-electron transfer process and H_2O_2 production. Although ZIF-8 lacks catalytic activity towards the ORR, its passive role as an in situ O_2 reservoir not only enhanced the measured current response, but also extended the region of electrochemical potential under kinetic control.

Introduction

Worldwide growing demand for clean energy is the driving force behind a great deal of efforts devoted to enhancing the oxygen reduction reaction (ORR) performance in hydrogen combustion cells and other energy conversion devices.[1–3] Unfortunately, this electrochemical reaction of great technological importance has sluggish kinetics and therefore requires the use of catalysts, among which Pt-group metals or PGMs stand out. The high demand and low availability of PGMs triggered an intense research activity oriented towards identifying adequate and cost-effective alternatives.[4–6] In order to accumulate competitive advantages, the design of these alternative electrode architectures are often complex and, in general, consist of multiple layers of functional coatings, which we identify as "active" or "passive", depending on whether or not they exhibit catalytic activity for the reaction of interest.

Considerable attention has been paid to electroactive thin films produced with conductive polymers (CPs) that, in addition to their cost-effectiveness, are characterized by high conductivity, chemical stability and catalytic activity.[7–11] Among CPs, poly(3-aminobenzylamine-co-aniline) or P(ABA–ANI) has been recently shown to mediate the ORR in neutral solutions, enabling applications in biocompatible conditions.[12] Although the electrochemical response of P (ABA–ANI) thin films towards the ORR has already been reported, there are several unknown aspects of the actual mechanism operating on this active functional coating.

A passive functional coating would be any material that improves the current response of the system by controlling the availability and diffusion of reagents and products in the vicinity of the electrode surface. Metal Organic Frameworks or MOFs are interesting materials in this regard.[13,14] To name a few relevant examples, an increase in performance has been reported for Li–ion, Li–S and Li–O_2 batteries upon the inclusion of MOFs into their architecture; in each case, the authors attribute this improvement to increased availability of reagents.[15–19] Moreover, Rafti et al.[20] and Fenoy et al.[21] have reported improvements in the current response of P(ABA–ANI)-coated electrodes after including ZIF-8 MOF. This MOF belongs to the Zeolitic Imidazolate Frameworks subclass which consists of a network of metal ions (usually Co^{2+} or Zn^{2+}) tetrahedrally coordinated by imidazole-based ligands.[22] In particular, ZIF-8 is formed by Zn^{2+} ions and 2-methylimidazolate linkers, features formidable physical-chemical stability at intermediate pH and selective O_2 absorption over N_2, in a 6:1 ratio.[23] Although these passive functional coatings do not display catalytic activity, their ability to alter the reaction mechanism should not be ruled out (see Figure 1 below).

Not only it is highly relevant to determine the electrochemical response of these novel hybrid electrodes, but also to assess how their design impacts on the reaction pathway. Our motivation derives from the fact that the ORR can occur via several possible mechanisms, depending on the nature of the

[a] F. C. D. López, J. A. Allegretto, W. A. Marmisollé, O. Azzaroni, M. Rafti, D. Grumelli
Instituto de Investigaciones Fisicoquímicas Teóricas y Aplicadas (INIFTA), UNLP-CONICET
La Plata
Buenos Aires 1900 (Argentina)
E-mail: mrafti@quimica.unlp.edu.ar
doris@inifta.unlp.edu.ar
[b] A. I. Bertoni
Instituto Interdisciplinario de Ciencias Básicas (ICB), UNCuyo-CONICET
Padre Jorge Contreras 1300
Mendoza 5502 (Argentina)

Supporting information for this article is available on the WWW under https://doi.org/10.1002/cctc.202201015

This publication is part of "Catalysis in Latin America". Please check the ChemCatChem homepage for more articles in the collection.
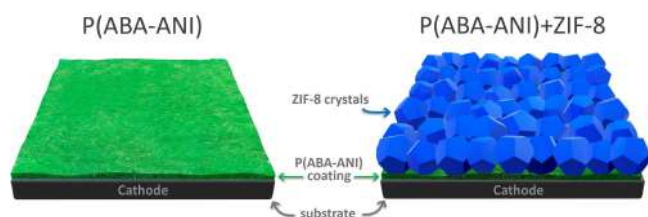
Figure 1. Representation of the electrodes used in this work: single P(ABA–ANI) (left) and P(ABA–ANI)+ZIF-8 (right) coated electrode.

catalyst and the conditions employed (e.g. pH).[24–26] Although the spectrum of mechanisms is broad, kinetic studies have established three main pathways:[27,28]

- Direct or dissociative pathway, involving the transfer of four electrons and the generation of H_2O (in acid medium) or OH^- (in alkaline medium).
- Indirect or associative pathway, involving the transfer of two electrons and the generation of H_2O_2.
- Multi-step indirect pathway, involving the generation and reduction of H_2O_2.

In this work, we aim to characterize the operating mechanism for the ORR on P(ABA–ANI) thin films at neutral pH, and to assess how the inclusion of a ZIF-8 microcrystals layer to the electrode's architecture impacts on the electrocatalytic performance.

Results and Discussion

Synthesis and characterization of electrochemically active and passive films: We synthesized P(ABA–ANI) thin films on conductive Au substrates via electropolymerization (see details in experimental section) and characterized its electrochemical response in neutral and acidic medium. The obtained response was in line with previous reports[12,20,21] (see supporting information for details, Figure SI.2, SI.3.a and SI.3.b). We determined that, after 20 cycles of electropolymerization, the film had a thickness of approximately 8.5 nm and a root mean square roughness (σ rms) of 2.49 nm or mean roughness (σ_a) of 1.96 nm (see the full mofological analysis of the P(ABA–ANI) film in the supplementary information, section 4). On P-(ABA–ANI) modified electrodes, we grew a second layer of ZIF-8 microcrystals, resulting in P(ABA–ANI)+ZIF-8 systems. XRD results confirm the successful inclusion of ZIF-8 into the hybrid electrode architecture, as seen in Figure SI.5. Via SEM and AFM experiments, we were able to determine the morphology of the included ZIF-8 phase. We observed microcrystals with diameters below 500 nm, exhibiting one of the following two morphologies: rhombic dodecahedra with truncated corners and, in a smaller proportion, rhombic dodecahedra. These two morphologies correspond to different stages in ZIF-8 crystal growth[29] (see full analysis in supporting information, Figure SI.6).

Electrocatalytic activity of hybrid electrodes towards ORR: The cathodic sweep for the P(ABA–ANI)-coated and P-(ABA–ANI)+ZIF-8 electrodes in O_2-saturated HEPES buffer are

shown in Figure 2. Both electrodes showed electrochemical activity towards the ORR, with a cathodic peak centered at −0.35 V. In both cases there is also a small shoulder centered at −0.65 V, which is more evident for the bare P(ABA–ANI)-coated electrode; we ascribe this feature to a second reduction process that we will address later. The addition of ZIF-8 led to an increase in the current density (of ~30%), which could be attributed to its already suggested role as an in situ O_2 reservoir.[20,21] We confirmed the passive role of the ZIF-8 layer with the persistence of the onset potential value at ~−0.15 V (see Figure 2). The inset in Figure 2 shows the chronoamperometric responses for the bare P(ABA–ANI) and P(ABA–ANI)+ZIF-8 electrodes at −0.35 V for 300 seconds, where the current density of the doubly modified electrode decays more slowly in line with the already suggested role of ZIF-8 as an O_2 reservoir, as discussed above.

Koutecky–Levich analysis: The Koutecky–Levich equation models the experimentally determined current density (j) as a function of the rotational speed (ω) of the RDE:

$$\frac{1}{j} = \frac{1}{j_k} + \frac{1}{j_d} = \frac{1}{j_k} + \frac{1}{B_L \omega^{1/2}} \tag{1}$$

$$B_L = 0.62 \, n \, F \, \beta \tag{2}$$

$$\beta = D^{2/3} \, v^{-1/6} \, C \tag{3}$$

where F is the Faraday constant, n is the global number of transferred electrons and β is a parameter that exclusively depends on the reagent and the medium solution (D is the diffusion coefficient of the electroactive species in the medium, v is the kinematic viscosity of the medium, C is the analyte concentration). As detailed in the supplementary information,
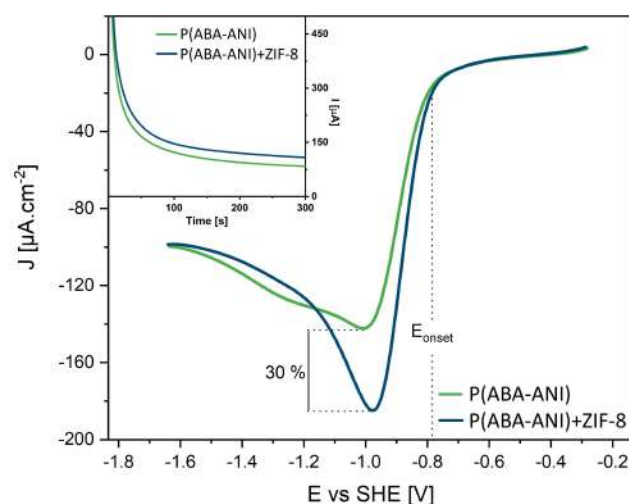

Figure 2. Cathodic sweep for the P(ABA–ANI) (green line) and P(ABA–ANI)-+ZIF-8 (blue line) surfaces in in O_2-saturated HEPES buffer at 0.10 V.s^{-1}. The blue dashed line follows the baseline of the P(ABA–ANI)+ZIF-8 response in order to highlight the small shoulder at −0.65 V. Inset: chronoamperometric response for both P(ABA–ANI) (green line) and P(ABA–ANI)+ZIF-8 (blue line) surfaces (−0.35 V).

ChemCatChem

Research Article
doi.org/10.1002/cctc.202201015

**Chemistry
Europe**
European Chemical
Societies Publishing

we determined the β parameter for the HEPES/O_2 buffer via the ORR on a polycrystalline Pt electrode at neutral pH.

We performed a linear scan voltammetry (LSV) at 0.02 V/s for both bare P(ABA−ANI) and P(ABA−ANI)+ZIF-8 electrodes in O_2-saturated HEPES buffer, as shown in Figure 3a. Each of the LSV curves, acquired at different rotational speeds, reaches, as expected, a current density plateau[30].

From the Koutecky–Levich analysis we were able to calculate n as a function of the applied potential, as shown in Figure 3.b for P(ABA−ANI) and P(ABA−ANI)+ZIF-8 modified electrodes. Both systems reached a maximum n value of 2.09, from −0.7 V to −1.0 V. This value implies that most active sites on the modified electrodes are catalyzing the ORR via a $2e^-$ pathway that involves the production of H_2O_2 as main product. The presence of H_2O_2 was confirmed by means of a colorimetric technique (see in supporting Information, section S7). The

dissociative pathway not being preferred may be due to a kinetically impeded electroreduction of the intermediate product, H_2O_2; Doubova et al. provided a similar explanation for a related system.[31] This is consistent with other kinetic studies reported for the ORR on PANI- and PABS-coated electrodes. PANI is the homopolymer of aniline (i.e. the electrocatalytic monomer in the active copolymer used in this work) and catalyzes the ORR via the associative pathway in acidic media.[8] The poly-aminosulfonic acid, PABS, is the homopolymer of an aniline derivative that was also found to exhibit an associative mechanism in neutral media.[32]

Values of n being slightly higher than 2 could be related to the reduction reaction of a small fraction of the produced H_2O_2, a process that would produce OH^- as a final product and a shoulder at −0.65 V in Figure 2. The limit value of n appears to be independent of the presence of ZIF-8. However, the plateau value at $n \approx 2$ is only maintained up to −0.7 V for bare P(ABA−ANI), while for the hybrid P(ABA−ANI)+ZIF-8 electrodes n remains constant for a wider potential range, holding up to −0.35 V. The ZIF-8 decorated electrode being able to reach the limit value of n at lower applied potentials can be attributed to the higher oxygen availability for the ORR conferred by this additional passive coating. This increased availability of reagents, mediated by ZIF-8, would result in an extension of the potential region where the diffusional current is the main contribution to the total current [Equation (3)]. The same conclusion can be inferred indirectly by visual inspection of Koutecky–Levich plots (Figure 3b inset); while slopes for the bare P(ABA−ANI) electrode remain non-parallel, slopes for P(ABA−ANI)+ZIF-8 electrode are already stabilized. This also implies that for P(ABA−ANI)+ZIF-8 there is a higher oxygen availability for the ORR, thus confirming the role of ZIF-8 as an in situ reservoir. The shaded bands in Figure 3.b correspond to the 99% confidence intervals associated with the calculation of n, and are derived from the least squares fit of the Koutecky–Levich expression to RDE experimental data. For applied potentials below the onset, computed n values bear no physical meaning and therefore are not shown.

Tafel analysis: We determined the charge transfer current density j_k from the y-intercept of the Koutecky–Levich linear fit, as detailed in Section 3.3. Considering that the ORR on the modified electrodes occurs via the associative pathway ($n=2$), to calculate the overpotential η we employed a value of $E_0=$ 0.28 V, which corresponds to the reduction of O_2 to yield H_2O_2 at pH 7.[33]

In Figure 4, we can see that Tafel plots for the P(ABA−ANI) and P(ABA−ANI)+ZIF-8 electrodes have a close resemblance. The strong similarity can be seen as another confirmation that the addition of ZIF-8 is not altering the electron transfer process. The presence of two different slopes, with a break at $\eta=-0.3$ V, implies a change in the reaction-determining step of the ORR mechanism with increasing overpotential.[34] The segments at low overpotentials have Tafel slopes of −0.107 V/dec for P(ABA−ANI) and of −0,105 V/dec for P(ABA−ANI)+ZIF-8; past the break at $\eta=-0.3$ V, slopes become slightly steeper with values of −0.155 V/dec and −0.161 V/dec, respectively. We found that our results are in line with those previously reported
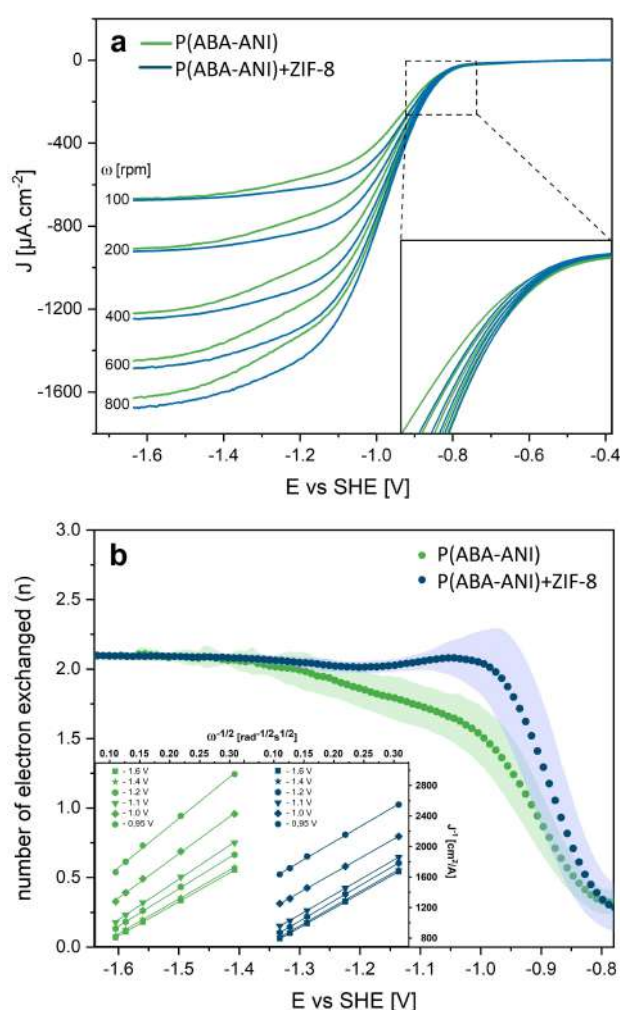
Figure 3. a. LSV responses for Au RDEs covered with P(ABA−ANI) (green line) and P(ABA−ANI)+ZIF-8 (blue line) at different rotational speeds. Inset: zoom to highlight the onset area. **b**. Plot of number of electrons transferred in the ORR vs. E for P(ABA−ANI) (green line) and P(ABA−ANI)+ZIF-8 modified electrodes; the colored regions enclose the 99% confidence intervals, computed from the standard deviation of the fit to the Koutecky–Levich equation, at each potential. Inset: Koutecky–Levich plots $(1/j_k)$ vs. $(1/\omega^{1/2})$ for P(ABA−ANI) (green lines) and P(ABA−ANI)+ZIF-8 (blue lines) at different potentials: −0.035 V, 0.4 V, −0.5 V, −0.6 V, −0.8 V and −1.0 V).

ChemCatChem

Research Article
doi.org/10.1002/cctc.202201015

Chemistry
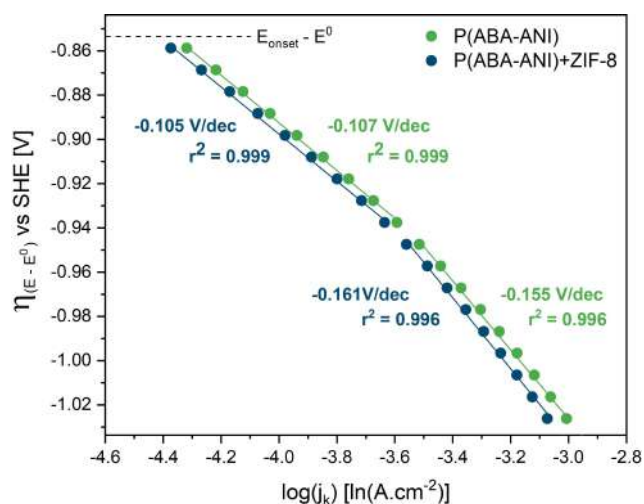**Europe**
European Chemical
Societies Publishing

Figure 4. Tafel plots for P(ABA−ANI) (green lines) and P(ABA−ANI)+ZIF-8 (blue lines) modified electrodes at pH 7. Tafel slopes values and their fit quality (r^2) are indicated in each region for each system.

for the ORR on polycrystalline Pt, at a similar pH (−0.120 V/dec and −0.175 V/dec, at pH 6).[35] At overpotentials close to the onset, the Tafel slope would appear to be near the theoretical value corresponding to the first electronic discharge step, after the binding of O_2 to the active site M ($MO_2 + e^- \rightarrow MO_2^-$); this suggests a rate-determining step with $n_\alpha = 1$ for low overpotentials. The difference in slopes may also be explained by the microkinetic model for Tafel slopes. According to this model, the observed change in slope at $\eta = -0.3$ V could be due to a change in the degree of coverage (θ) of the active sites with oxygen species, which is dependent on the applied potential.[36] According to this model, steep slopes are expected for low degrees of coverage, and vice versa.[37–39]

The exchange current density (j_0) was obtained from the y-intercept of the Tafel linear fit. This kinetic parameter indicates the rate of the reaction at thermodynamic equilibrium, and its value depends on the details of the electrochemical catalytic reaction.[40] We found j_0 to be independent of the presence of ZIF-8; its value of 3.10^{-7} A.cm^{-2} at low overpotentials rises by an order of magnitude (to 3.10^{-6} A.cm^{-2}) after the change in the reaction-determining step at $\eta = -0.3$ V.

Analysis of the different contributions to the measured current: As we discussed in the Koutecky–Levich and Tafel analyses of the previous sections, the mechanistic and kinetic parameters for the ORR on P(ABA−ANI) electrodes did not change after the inclusion of ZIF-8 into the electrode architecture. Although ZIF-8 lacks catalytic activity towards the ORR, its inclusion led to a remarkable increase in the measured current density and allowed reaching the limit value of n at smaller overpotentials. As discussed above, this is related to the role of ZIF-8 as an in situ O_2 reservoir. In other words, if the presence of ZIF-8 increases local concentration of O_2 near active sites, then ORR diffusional-related limitations should decrease. To test such hypothesis, we compared plots corresponding to the relative contributions to measured current, as a function of

applied potential, based on the Koutecky–Levich equation [Equation (1)]:

$$1 = \frac{j}{j_k} + \frac{j}{j_d} \tag{4}$$

As the charge and mass transfer contributions of Equation (4) are expressed as relative to the total current, terms are limited to take values between 0 and 1, and its sum should be equal to 1. This normalization allows comparison between different experiments, as the relative contributions are independent of the maximum current response exhibited by each particular system. The relative kinetic contribution term was calculated as the ratio between the measured current (j) and the charge transfer current (j_k) taken from the y-intercept of Koutecky–Levich fits, while the relative diffusional contribution term (j/j_d) was derived from Equation (4):

$$\frac{j}{j_d} = 1 - \frac{j}{j_k} \tag{5}$$

In Figure 5a, we used the unmodified bare gold electrode as a reference system to show that relative contributions plots allow straightforward identification of the regions of applied
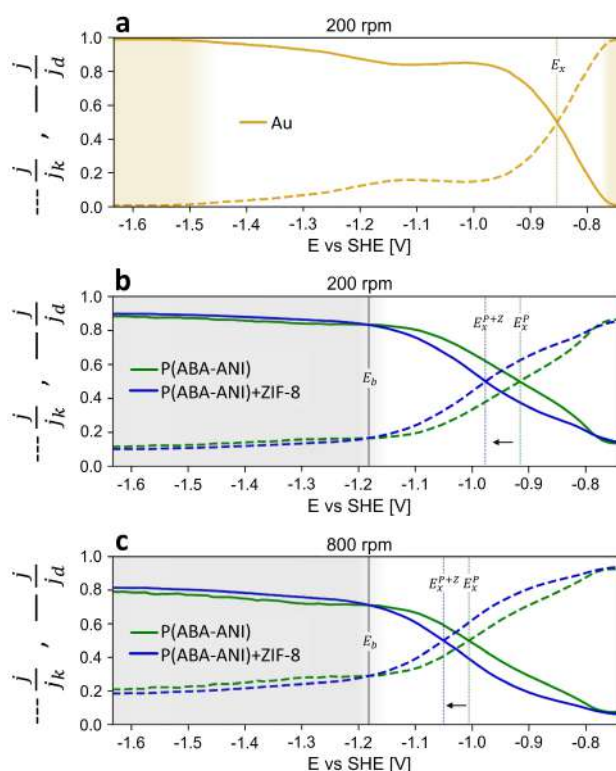

Figure 5. Variation of the charge (j/j_k dash lines) and mass (j/j_d full lines) transport contributions to the measured current, as a function of the applied potential during the ORR for: a) unmodified bare gold electrode, b and c) P(ABA−ANI) (green line) and P(ABA−ANI)+ZIF-8 (blue line) modified electrodes. Values of j_k were obtained from the y-intercept of the Koutecky–Levich linear fit of section 3.3, while values of j_d were adjusted to ensure the normalization condition of Equation (4).

potential under either kinetic or diffusional control. In relative contributions plots, we refer to the value of applied potential where the relative contributions become equal as the "crossover potential" (E_x). Notice how E_x marks the change of dominance between the relative contributions to the measured current: moving towards more negative values of the applied potential, E_x marks the transition from a domain under kinetic control into a region of applied potential where the reaction is under diffusional control. For the bare gold surface, we can even recognize small subdomains where the measured current is either purely diffusional or purely kinetic (see the shaded regions in Figure 5.a).

In panels b and c of Figure 5, we show overlapped relative contributions plots for the P(ABA–ANI) and P(ABA–ANI)+ZIF-8 modified electrodes, corresponding to RDE experiments with rotational speeds of 200 and 800 rpm, respectively. The first thing to notice is that adding functional coatings to the bare gold electrode resulted in the absence of regions of applied potential under full kinetic or full diffusional control. A related observation can be made in the inset of Figure 3a, where an increase in the measured current can be seen when rotational speed is incremented, in a region of overpotential that is typically considered to be under full kinetic control.[41] As the major change is observed after the addition of the P(ABA–ANI) coating layer, we hypothesize that the absence of regions where the current is purely kinetic or purely diffusional can be ascribed to i) the polymer itself acting as a three-dimensional physical obstacle to the free diffusion of the reactant, thus resulting in a local decrease of O_2 concentration around the active sites inside the polymer film; or to ii) charge transfer limitations due to a deficient electric/ionic transport within the polymer film. Interestingly, differences in the kinetic performance on Au and Au/P(ABA–ANI) in terms of the relative contributions remain the same after anchoring the ZIF-8 layer. This implies that the MOF does not hinder the electronic/ionic transport within the polymer film. This is also in agreement with previous studies by cyclic voltammetry in which it has been shown that the presence of the MOF coating on the electroactive polymer does not worsen the electronic transport within the polymer film, as revealed by the coincidence of the voltammetric current previous to the ORR.[20]

Also in the plots of Figure 5b–c, it can be seen that E_x shifts towards more negative potentials with the addition of ZIF-8 ($E_x^P \rightarrow E_x^{P+Z}$) and with the increase of the electrodes' rotational speed. These shifts can be caused either by an increase of the charge transfer contribution or by a decrease on the diffusional contribution; the former being linked to catalysis-related aspects and the latter to the mass transfer of the involved species. For the particular systems under study, it is worth emphasizing that any observed change in the relative kinetic contribution term actually arises from variations of the mass transfer current, as we determined almost identical charge transfer currents for the P(ABA–ANI) and P(ABA–ANI)+ZIF-8 electrodes (see Figure SI.7.d in supporting information), which is consistent with ZIF-8 not being an ORR catalyst.

If we take into account that the decoration with ZIF-8 microcrystals keeps unaltered the electrocatalytic activity of the P(ABA–ANI) coated electrodes, then the shift of crossover potentials towards more negative values should be necessarily caused by a decrease of the diffusional limitations. According to Levich's equation, increasing the local concentration of the analyte increases the diffusional current, which in turn decreases the diffusional contribution term. A local increase in the analyte concentration can be obtained by improving its supply to the electrode; this can be done, for example, by increasing the rotational speed of the electrode or by attaching a reservoir that pre-concentrates the reactant close to the active sites. In other words, coating the electrode with ZIF-8, and increasing its rotational speed, provokes a shift in E_x towards higher overpotentials, extending the region of potential under kinetic control, which is in line with our hypothesis regarding the increased local availability of O_2 yielding a reduction of the diffusional limitations. In Figure 5b–c, a reduction of the diffusional limitations is seen as the curve corresponding to the relative diffusional contribution (solid line) dropping after the addition of ZIF-8 (from green to blue) for potentials surrounding E_x.

Although it would be reasonable to expect that increasing the local O_2 concentration would lead to a decrease of the diffusional contribution term for all values of the applied potential, Figure 5 shows that this is not the case. We detected a certain value of applied potential that we refer to as the "barrier potential" (E_b), above which the relative diffusional contribution becomes slightly higher for the ZIF-8 containing electrode (grey background). This value of applied potential was found to be independent of the electrode's rotational speed (fixed at -0.56 V for 100–800 rpm), indicating that its particular value may be linked to a purely kinetic event. For very high overpotentials, past E_b, the presence of the ZIF-8 layer appears to be imposing extra diffusional limitations in comparison to the electrode modified with P(ABA–ANI) only. Although we are unaware of the actual reasons behind this effect, we hypothesize that this could be related to a decrease in the local availability of O_2 that occurs only at very high overpotentials; for example, this could be due to the accumulation of H_2O_2 in the interlayer region between the active layer of P(ABA–ANI) and the passive layer of ZIF-8 microcrystals. This presumed second passive role of ZIF-8 as a physical barrier, if true, would be preventing the free diffusion of the ORR product into the bulk of the solution, thus hindering the local replenishment of the reagent. However, while determining the true origin of E_b may be of interest, it is certainly beyond the intended scope of this work.

Conclusion

We determined that on P(ABA–ANI)-coated electrodes the ORR occurs (at neutral pH) via an associative pathway, involving a two-electron transfer process and the production of H_2O_2. We were also able to determine that including a layer of ZIF-8 microcrystals led to a remarkable increase in the measured current, without altering the original ORR mechanistic pathway or its main kinetic parameters. Although ZIF-8 lacks catalytic

ChemCatChem

Research Article
doi.org/10.1002/cctc.202201015

**Chemistry
Europe**
European Chemical
Societies Publishing

activity towards the ORR, we established that its presence in the electrode architecture extends the region of applied potential that is under kinetic control, due to a reduction in the diffusional limitations resulting from an increased local availability of O_2. In other words, the main passive role of ZIF-8 is to act as an in situ reservoir that pre-concentrates O_2 near the active sites.

Experimental Section

Reactant. Aniline (ANI), 3-aminobenzylamine (ABA), $Zn(NO_3)_2 \cdot 6H_2O$, 2-methyl-imidazole (HmIm) and $C_8H_{17}N_2NaO_4S$ (HEPES) were purchased from Sigma-Aldrich. H_2SO_4 and NH_4OH were purchased from Anedra. Methanol and H_2O_2 were purchased from Cicarelli. KCl salt was purchased from Biopack. Prior to use, aniline was purified by distillation in vacuum; the rest of the reagents were used as receive. All aqueous solutions were prepared with ultrapure water (Milli-Q, $R = 18.2 M\Omega$).

Instruments. All electrochemical experiments were performed in a standard three-electrode cell connected to an AUTOLAB PGSTAT302N potentiostat (Metrohm); using the NOVA 2.1 software. The working electrodes were constructed as indicated in sections "Preparation of the conductive substrate" and "Modification of working electrodes". A Pt wire served as a counter electrode. All cell potentials were measured with respect to an Ag/AgCl 3 M KCl reference electrode and for ease of comparison with other catalytic systems are referenced to the standard hydrogen electrode (SHE). For hydrodynamic tests we have employed a rotational speed controller from Princeton Applied Research (model 636). Coating thickness measurements were determined by an atomic force microscope (AFM), Dimension Icon (Bruker), controlled via the NanoScope V software. Tips FESP–V2 (Bruker) with a force contact of 2,8 N/m were used. Scanning electron microscopy (SEM) images were taken on a Zeiss equipment model GeminiSEM 500, under ambient conditions. X-ray diffraction (XRD) patterns were generated on a Bruker D8-Advance (Bragg-Brentano geometry) using a Cu–Kα1 Ge(111) Monochromator, and data was collected on a Våntec detector. The calculated XRD patterns were obtained from the Cambridge Crystallographic Data Centre (CCDC).

Preparation of the conductive substrate. A glass substrate coated with a Ti/Au (10 nm/200 nm thick respectively) was used as bare conductive substrate. Ti layer improve Au adhesion. Prior to use, the working electrodes were cleaned with basic piranha solution (NH_4OH:H_2O_2:H_2O 1:1:7) and then sonicated in ultrapure water. For kinetic experiments, Au and Pt rotating disk electrodes (RDE) (E3T series, Pine Research) were used; these electrodes consisted of polycrystalline metal disks, 5 mm in diameter, embedded in polytetrafluoroethylene (PTFE). Before use, these RDEs were polished on microfabric cloths from 1, 0.3 and 0.05 μm alumina paste, for 5, 15 and 45 min respectively, properly sonicated and rinsed with ultrapure water after every step. The cleaning process was monitored by cyclic voltammetry (CV).

Modification of working electrodes. The working electrodes were modified with two layers of functional coatings: P(ABA–ANI) and ZIF-8. The first layer consists on a nanofilm of the conductive polymer P(ABA–ANI). P(ABA–ANI) electropolymerization on conductive Au substrate was achieve by 20 cycles of CV between −0.15 V to 0.95 V vs Ag/AgCl, at 0.05 V.s^{-1} of 0.03 M ANI and 0.07 M ABA in acidic medium.[12] The electrochemical response of the polymeric material was evaluated with CV in acidic and neutral medium rinsed with ultrapure water prior to the experiment. The thickness of the P(ABA–ANI) nanofilm was determined with AFM,

by the tip-based scratching method.[42] In "contact" mode operation a window of 360 nm×720 nm was created by removing the material with the tip. After tip scratching procedure and image of 4 μm×4 μm with a resolution of 512×512 pixels was aquired in tapping mode was acquire in tapping mode in order to estimate the thickness of the thin film by a line profile along the edge of the window. After that, a second functional coating layer consist on microcrystals of the MOF ZIF-8 was added. The growth of ZIF-8 on the P(ABA–ANI) nanofilm was performed at room temperature, following the fast route reported by Cravillon et al. Shortly, methanolic solutions of 50 mM HmIm and 25 mM Zn(NO3)$_2$•6H2O were used. A complete reaction cycle between precursors requires approximately 40 min, according to Rafti et al.[20] The ZIF-8 coating layer was characterized by XRD, SEM and AFM. Due to our interest in using the P(ABA–ANI) + ZIF-8 films for the evaluation of ORR electrocatalytic and kinetics performance, we made use of a single cycle of synthesis of ZIF-8 microcrystals. Fenoy et al. observed that thick films of ZIF-8 generate a decrease in the catalytic currents due to a presumed impairment in the diffusion of dissolved O_2.[21] Only a thicker film was prepared by 10 cycles of synthesis in order to enhance the XRD signals for the crystal structure characterization. XRD data was captured in the 2θ range from 5° to 30° (major peak region), in steps of 0.02°. Figure SI.1 summarizes in a diagram the pair of modifications made resulting in a P(ABA–ANI) + ZIF-8 working electrodes.

Electrocatalysis and kinetic studies. The electrocatalytic activity toward the ORR for the modified electrodes was evaluated at pH 7 in 5 mM HEPES/0.1 M KCl aqueous solutions. Either CV or linear sweep voltammetry (LSV) experiments from 0.3 V to −1 V vs Ag/AgCl, at 0.01 V.s^{-1} were employed. Kinetic information was extracted from hydrodynamic voltammetry experiments with RDEs with rotational speeds (ω) of 100, 200, 400, 600 and 800 rpm.

Acknowledgements

Conflict of Interest

The authors declare no conflict of interest.

Data Availability Statement

The data that support the findings of this study are available in the supplementary material of this article.

[1] S. G. Peera, T. Maiyalagan, C. Liu, S. Ashmath, T. G. Lee, Z. Jiang, S. Mao, *Int. J. Hydrogen Energy* **2021**, *46 (4)*, 3056–3089.

[2] S. Hossain, A. M. Abdalla, S. B. Suhaili, I. Kama, S. P. Shaikh, M. K. Dawood, A. K. Azad, *J. Energy Storage* **2020**, *29*, 101386.

[3] N. Delaporte, E. Rivard, S. K. Natarajan, P. Benard, M. L. Trudeau, K. Zaghib, *Nanomaterials* **2020**, *10 (10)*, 1947.

[4] O. Lori, L. Elbaz, *ChemCatChem* **2020**, *12 (13)*, 3434–3446.

[5] M. Shao, Q. Chang, J. P. Dodelet, R. Chenitz, *Chem. Rev.* **2016**, *116 (6)*, 3594–3657.

[6] C. J. Yang, *Energy Policy* **2009**, *37 (5)*, 1805–1808.

[7] V. Guarino, S. Zuppolini, A. Borriello, L. Ambrosio, *Polymer* **2016**, *8 (5)*, 185.

[8] V. G. Khomenko, V. Z. Barsukov, A. S. Katashinskii, *Electrochim. Acta* **2005**, *50 (7–8)*, 1675–1683.

[9] A. G. MacDiarmid, *Rev. Mod. Phys.* **2001**, *73 (3)*, 701.

[10] A. Malinauskas, *Synth. Met.* **1999**, *107 (2)*, 75–83.

[11] C. K. Chiang, C. R. Fincher Jr., Y. W. Park, A. J. Heeger, H. Shirakawa, E. J. Louis, S. C. Gau, A. G. MacDiarmid, *Phys. Rev. Lett.* **1977**, *39*, 1098.

[12] W. A. Marmisollé, D. Gregurec, S. Moya, O. Azzaroni, *ChemElectroChem* **2015**, *2 (12)*, 2011–2019.

[13] O. M. Yaghi, N. W. Ockwig, H. K. Chae, M. Eddaoudi, J. Kim, *Nature* **2003**, *423 (6941)*, 705–714.

[14] M. Eddaoudi, J. Kim, N. Rosi, D. Vodak, J. Wachter, M. O'Keeffe, O. M. Yaghi, *Science* **2002**, *295 (5554)*, 469–472.

[15] Y. Han, P. Qi, X. Feng, S. Li, X. Fu, H. Li, Y. Chen, J. Zhou, X. Li, B. Wang, *ACS Appl. Mater. Interfaces* **2015**, *7 (4)*, 2178–2182.

[16] J. Zhou, R. Li, X. Fan, Y. Chen, R. Han, W. Li, J. Zheng, B. Wang, X. Li, *Energy Environ. Sci.* **2014**, *7 (8)*, 2715–2724.

[17] D. Wu, Z. Guo, X. Yin, Q. Pang, B. Tu, L. Zhang, Y. Wang, Q. Li, *Adv. Mater.* **2014**, *26 (20)*, 3258–3262.

[18] X. Zheng, Y. Li, Y. Xu, Z. Hong, M. Wei, *CrystEngComm* **2012**, *14 (6)*, 2112–2116.

[19] R. Demir-Cakan, M. Morcrette, F. Nouar, C. Davoisne, T. Devic, D. Gonbeau, R. Dominko, C. Serre, G. Férey, J.-M. Tarascon, *J. Am. Chem. Soc.* **2011**, *133 (40)*, 16154–16160.

[20] M. Rafti, W. A. Marmisollé, O. Azzaroni, *Adv. Mater. Interfaces* **2016**, *3 (16)*, 600047.

[21] G. E. Fenoy, J. Scotto, J. Azcárate, M. Rafti, W. A. Marmisollé, O. Azzaroni, *ACS Appl. Energ. Mater.* **2018**, *1 (10)*, 5428–5436.

[22] K. S. Park, Z. Ni, A. P. Côté, J. Y. Choi, R. Huang, F. J. Uribe-Romo, H. K. Chae, M. O'Keeffe, O. M. Yaghi, *Proc. Natl. Acad. Sci. USA* **2006**, *103 (27)*, 10186–10191.

[23] K. Díaz, M. López-González, L. F. del Castillo, E. Riande, *J. Membr. Sci.* **2011**, *383 (1–2)*, 206–213.

[24] D. T. Sawyer, G. Chiericato, C. T. Angelis, E. J. Nanni, T. Tsuchiya, *Anal. Chem.* **1982**, *54 (11)*, 1720–1724.

[25] A. Ricardo, S. Olaya, Thesis: Estudio de la reacción de reducción de oxígeno sobre electrodos mono cristalinos de platino modificados con películas delgadas de polianilina, Universidad Nacional de Colombia, Departamento de Química, **2012**.

[26] S. Rojas-Carbonell, K. Artyushkova, A. Serov, C. Santoro, I. Matanovic, P. Atanassov, *ACS Catal.* **2018**, *8 (4)*, 3041–3053.

[27] Y. Nie, L. Li, Z. Wei, *Chem. Soc. Rev.* **2015**, *44 (8)*, 2168–2201.

[28] A. A. Gewirth, M. S. Thorum, *Inorg. Chem.* **2010**, *49 (8)*, 3557–3566.

[29] C. Avci, J. Ariñez-Soriano, A. Carné-Sánchez, V. Guillerm, C. Carbonell, I. Imaz, D. Maspoch, *Angew. Chem.* **2015**, *127 (48)*, 14625–14629.

[30] F. Gloaguen, F. Andolfatto, R. Durand, P. Ozil, *J. Appl. Electrochem.* **1994**, *24 (9)*, 863–869.

[31] L. Doubova, G. Mengoli, M. M. Musiani, S. Valcher, *Electrochim. Acta* **1989**, *34 (3)*, 337–343.

[32] S. A. Kumar, S. M. Chen, *J. Mol. Catal. A* **2007**, *278 (1–2)*, 244–250.

[33] P. M. Wood, *Biochem. J.* **1988**, *253 (1)*, 287.

[34] Q. Li, X. Zhou, Z. Wei, G. Du, G. Zhang, N. Chen, *J. Rare Earth* **2019**, *37 (3)*, 282–286.

[35] S. Strbac, *Electrochim. Acta* **2010**, *56 (3)*, 1597–1604.

[36] T. Shinagawa, A. T. Garcia-Esparza, K. Takanabe, *Sci. Rep.* **2015**, *5 (1)*, 1–20.

[37] A. A. Gewirth, M. S. Thorum, *Inorg. Chem.* **2010**, *49 (8)*, 3557–3566.

[38] F. Tian, R. Jinnouchi, A. B. Anderson, *J. Phys. Chem. C* **2009**, *113 (40)*, 17484–17492.

[39] V. Rai, M. Aryanpour, H. Pitsch, *J. Phys. Chem. C* **2008**, *112 (26)*, 9760–9768.

[40] J. Zhang in *PEM Fuel Cell Electrocatalysts and Catalyst Layers*, Springer, London, **2008**, pp. 447–485.

[41] G. Yin, J. Zhang, *Rotating Electrode Methods and Oxygen Reduction Electrocatalysts*, **2014**, Elsevier.

[42] Y. Yan, S. Chang, T. Wang, Y. Geng, *Polymer* **2019**, *11 (10)*, 1590.